Dephasing-Induced Spin Relaxation in Ballistic Rashba Spin-Orbit Materials

Aron W. Cummings[1] and Stephan Roche[1,2]
[1]*ICN2 - Institut Català de Nanociència i Nanotecnologia, Campus UAB, 08193 Bellaterra (Barcelona), Spain*
[2]*ICREA, Institució Catalana de Recerca i Estudis Avançats, 08070 Barcelona, Spain*
(Dated: July 25, 2015)

We theoretically investigate spin dynamics in Rashba spin-orbit materials. In the limit of small momentum scattering (ballistic regime), spin relaxation is dictated by dephasing that arises from the combination of energy broadening and a non-uniform spin precession frequency. For graphene, we find that spin transport strongly depends on both the magnitude and direction of electron momentum, and that spin lifetimes are short even for modest energy scales, on the order of those seen experimentally. These results not only offer a deeper insight into the nature of spin dephasing and relaxation in graphene, but can also be used as a stepping stone for the investigation of spin dynamics in other forms of Dirac matter and two-dimensional systems exhibiting Rashba-induced spin split bands.

PACS numbers: 72.80.Vp, 72.25.-b, 71.70.Ej, 72.25.Rb

Introduction. Following the initial description of Rashba spin-orbit coupling (SOC) in two-dimensional (2D) electron gases [1], the understanding of band structure and spin dynamics in the presence of Rashba SOC has been essential for the proposal of spintronic devices such as the Datta-Das spin transistor [2], and for the prediction of fundamental physical phenomena such as the intrinsic spin Hall effect [3–5]. The properties of Rashba SOC allow for the manipulation of spin states by electrostatic means, making it possible to perform elementary operations and thus paving the way towards non-charge-based computing and information processing technologies [6]. Beyond traditional III-V semiconductor quantum wells – such as InAs or InGaAs – 2D graphene and monolayers of $\mathrm{MoS_2}$ and other group-VI dichalcogenides have recently raised a lot of interest. In addition to their predicted long spin lifetimes [7, 8], the possibility to harness proximity effects or to couple the spin and valley degrees of freedom makes these materials very interesting from both a fundamental and a technological perspective [9, 10]. From a practical point of view, understanding the relaxation mechanisms and spin lifetimes in clean materials is a prerequisite to realizing spintronic devices, since they determine the upper time and length scales on which spin devices can operate. In Rashba SOC materials, the spin lifetime is normally dictated by the Dyakonov-Perel (DP) mechanism [11], where SOC induces spin precession of charge carriers. After many scattering events the randomization of the precession leads to dephasing and a loss of the spin signal, with a spin relaxation time $\tau_s \propto 1/\tau_p$ (τ_p is the momentum scattering time). This scaling behavior contrasts with the Elliot-Yafet (EY) mechanism [12], for which $\tau_s \propto \tau_p$. The EY mechanism is usually at play in disordered metals, but its contribution in the presence of Rashba SOC has been proposed for graphene [13].

Rashba SOC in graphene is predicted to be small, on the order of μeV [14], leading to theoretical spin lifetimes in the micro- to millisecond range [7]. In contrast, experimental values in graphene range from a few hundred ps to a few ns for non-local Hanle measurements [15]. Various extrinsic mechanisms have been proposed to explain this discrepancy, including strain deformations [16], adsorbed metallic adatoms [17, 18], or magnetic resonances [19]. In most of the experiments and theories, and whatever the assumed relaxation mechanism (either DP or EY), the loss of spin polarization is inherently driven by impurity-induced momentum scattering, and is applicable to the situation where $\tau_s \gg \tau_p$. However, in materials with long mean free path, impurity scattering might cease to dominate the spin relaxation. To date, there is a lack of theoretical description of spin decoherence in such a regime, where charges can propagate ballistically over long distances.

This Letter presents a study of spin dynamics in Rashba SOC materials, in the limit of vanishing momentum scattering. We find that spin relaxation is induced by dephasing arising from energy broadening in combination with a nonuniform spin precession frequency. Using graphene as a case study, we show that its particular spin-split band structure can yield short spin lifetimes, even for modest values of energy broadening and Rashba SOC. τ_s is also shown to be strongly anisotropic with respect to the direction of charge propagation. Finally, τ_s exhibits a characteristic "inverted-W" shape as a function of charge density, mediated by the characteristics of the Rashba spin-split band structure.

Spin relaxation in clean systems. When momentum scattering becomes negligible, spin relaxation can arise from quantum dephasing, where an oscillating signal loses strength due to mixing with other signals of different phase or frequency. The spin of a charge carrier will precess around an effective magnetic field $\vec{B}_{eff}$ induced by the SOC. If the magnitude or direction of $\vec{B}_{eff}$ depends on the energy or momentum of the charge carriers, and if they occupy a distribution of energies or momenta, then the total spin signal will consist of a mix of frequencies and phases, and dephasing will occur. To see this more explicitly, consider the example shown in Fig. 1. Here we assume that the spin precession frequency in an arbitrary system varies linearly with energy, $\omega(E) = \omega_0 + \alpha E$. We also assume that the charge carriers occupy a Lorentzian distribution in energy, $\mathcal{L}(E) = \eta/[\pi \cdot (E^2 + \eta^2)]$, where η is the half-width at half-maximum (HWHM). It is straightforward

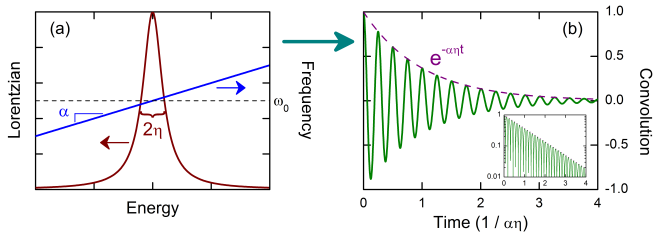

FIG. 1. (color online) (a) Convolution of an energy-dependent spin precession frequency (right axis) and a Lorentzian energy broadening (left axis). The HWHM of the Lorentzian is η, and the variation of the spin precession freqency is α. (b) This yields an exponentially-decaying cosine, with frequency ω_0 and decay time $1/\alpha\eta$.

to show that the total spin signal is

$$s(t) = \mathcal{L}(E) \circ \cos(\omega(E)t) = e^{-\alpha\eta t} \cdot \cos(\omega_0 t), \qquad (1)$$

where $\circ$ represents the convolution integral [20]. In general, Eq. (1) indicates that the combination of energy broadening and nonuniform spin precession leads to a decay of the spin signal due to dephasing, with a relaxation rate proportional to both the broadening η and the variation of the precession α. For a continuous distribution of charge carriers the decay is irreversible, i.e., the magnitude of the signal will never recover to its original value. In reality, a finite number of charge carriers will occupy a discrete set of energies, but this will also give an irreversible decay if the carriers are randomly distributed in energy. It is only for the case of a fully commensurate set of frequencies that the decay becomes reversible. For example, if the integral in Eq. (1) were replaced with a uniform sum, then the spin signal would exhibit a recovery time proportional to $1/\Delta E$, where ΔE is the uniform energy spacing. We also note that the decay is not necessarily exponential, but rather depends on the broadening function and the variation of the precession frequency. For example, replacing the Lorentzian in Eq. (1) with a Gaussian distribution gives a time decay of $\exp(-(\alpha\sigma t)^2/2)$, where σ is the standard deviation [20], while a Fermi distribution yields a decay of $\xi t/\sinh(\xi t)$, where $\xi = \alpha\pi kT$ and kT is the thermal energy [21].

Band structure of graphene with SOC. Since a nonuniform precession frequency can lead to spin relaxation in a clean system, we now examine the band structure of graphene in the presence of SOC. Considering a single π-orbital per carbon atom, the tight-binding Hamiltonian of this system is

$$\hat{H} = -t\sum_{\langle ij\rangle} c_i^\dagger c_j + i\frac{2}{\sqrt{3}}V_I \sum_{\langle\langle ij\rangle\rangle} c_i^\dagger \vec{s}\cdot(\vec{d}_{kj}\times\vec{d}_{ik})c_j + iV_R\sum_{\langle ij\rangle} c_i^\dagger \vec{z}\cdot(\vec{s}\times\vec{d}_{ij})c_j, \qquad (2)$$

where $\vec{s}$ are the Pauli spin matrices, t is the nearest-neighbor hopping, V_I is the intrinsic SOC, and V_R is the Rashba SOC, induced by a transverse electric field or a substrate [22]. Putting Eq. (2) into the spin+pseudospin basis and taking the

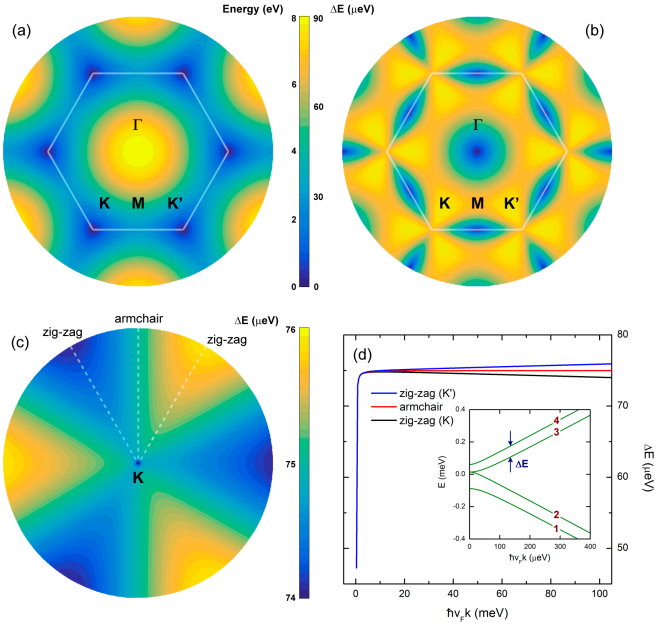

FIG. 2. (color online) Band structure of graphene with SOC. (a) The conduction band and (b) the spin splitting of the conduction band over the entire Brillouin zone. (c) Spin splitting of the conduction band near the K point. (d) Splitting of the conduction band near the K and K' points for the armchair and zig-zag directions. Inset: slice of the band structure near the K point (bands are labeled 1 to 4).

Fourier transform yields

$$\hat{H} = \begin{bmatrix} \beta & \kappa & 0 & i\gamma_+ \\ \kappa^* & -\beta & -i\gamma_-^* & 0 \\ 0 & i\gamma_- & -\beta & \kappa \\ -i\gamma_+^* & 0 & \kappa^* & \beta \end{bmatrix}, \qquad (3)$$

where $\kappa = -te^{ik_y\cdot 2b/3}\cdot[1+2e^{-ik_y b}\cos(k_x a)]$, $\gamma_\pm = V_R\cdot e^{ik_y\cdot 2b/3}\cdot[1+2e^{-ik_y b}\cos(k_x a \pm 2\pi/3)]$, $\beta = -V_I\cdot[2\sin(2k_x a) - 4\cos(k_y b)\sin(k_x a)]$, k_x and k_y are the momenta along the x- and y-directions, $a = \sqrt{3}/2\cdot a_{cc}$, $b = 3/2\cdot a_{cc}$, and a_{cc} is the carbon-carbon distance [23, 24].

In Fig. 2 we plot the band structure of this system, assuming t = 2.7 eV, V_I = 2.31 μeV, and V_R = 25 μeV [14]. Figure 2(a) shows the conduction band over the entire Brillouin zone, with the characteristic Dirac cones at the six corners and trigonal warping appearing at higher energies. To see the impact of SOC, in Fig. 2(b) we plot the spin splitting of the conduction band over the entire Brillouin zone. The splitting is zero at the Γ and M points. What is most interesting, however, is the splitting near the K and K' points. A zoom of this is shown in Fig. 2(c) around the K point, and highlights a highly nonuniform and anisotropic splitting. This is shown in more detail in Fig. 2(d), where the splitting is plotted as a function of momentum along the zig-zag and armchair directions for both the K and K' valleys. Along the armchair direction, the splitting increases rapidly away from the Dirac point and saturates at a constant value. However, along the zig-zag direction the splitting does not saturate, but instead exhibits a

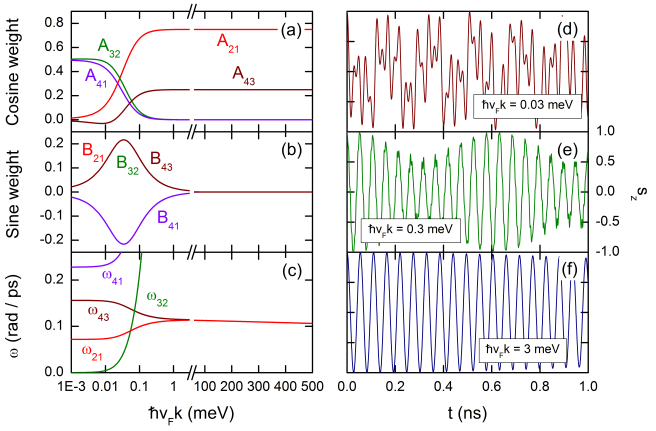

FIG. 3. (color online) Spin dynamics in graphene with SOC. (a) Cosine weights, (b) Sine weights, and (c) Precession frequency vs. momentum k, starting from the K valley and moving along the zig-zag direction. (d)-(f) Time-dependent spin polarization for selected values of k. The spin is projected along the z-axis.

slower variation after the initial rapid rise. As we will show in the next sections, this complex and nonuniform behavior is responsible for the fast spin dephasing and relaxation that we can observe in this clean graphene system.

Spin dynamics of graphene with SOC. To understand the connection between the band structure and spin relaxation, we first explicitly consider the connection between the band structure and the spin dynamics of charge carriers in a clean system. Starting with $\hat{H}|\phi_i\rangle = \epsilon_i|\phi_i\rangle$, where ϵ_i and $|\phi_i\rangle$ are the eigenvalues and eigenvectors of $\hat{H}$, the time-dependent spin polarization of an initial state $|\psi_0\rangle$ can be written as

$$\vec{p}(t) = \sum_i \vec{A}_{ii} + \sum_{i>j}[\vec{A}_{ij}\cos(\omega_{ij}t) + \vec{B}_{ij}\sin(\omega_{ij}t)], \quad (4)$$

where $\omega_{ij} = (\epsilon_i - \epsilon_j)/\hbar$, $\vec{A}_{ij}(\vec{B}_{ij})$ is the real (imaginary) part of $\langle\psi_0|\phi_i\rangle\langle\phi_i|\vec{s}|\phi_j\rangle\langle\phi_j|\psi_0\rangle$, and the sums run over all eigenstates at a given momentum k. The spin polarization consists of two terms – a constant term that depends on the polarization of each band, $\langle\phi_i|\vec{s}|\phi_i\rangle$, and an oscillating term whose frequencies are determined by the splitting between the bands, $\omega_{ij} = (\epsilon_i - \epsilon_j)/\hbar$. The weights $\vec{A}_{ij}$ and $\vec{B}_{ij}$ of the oscillating terms are determined by the spin-mediated overlap between bands, $\langle\phi_i|\vec{s}|\phi_j\rangle$.

As illustrated in Fig. 2, $\hat{H}$ depends strongly on the momentum k, and therefore so will the spin precession. This is shown more explicitly in Fig. 3, where we plot the weights, frequencies, and spin dynamics of charge carriers for different values of k along the zig-zag direction near the K point. Since the spin polarization of each eigenstate lies in the xy-plane, we consider polarization along the z-axis for the precession study. Fig. 3 show two different regimes. At large values of k, the spin dynamics is dominated by transitions between the two valence bands (bands 1 and 2, labeled in the inset of Fig. 2(d)) and the two conduction bands (bands 3 and 4). In this regime, ω_{21} and ω_{43} are nearly identical, leading to the regular oscillation in Fig. 3(f). At lower values of k, ω_{21} and ω_{43} diverge, resulting in the beating pattern shown in Fig. 3(e). As k approaches zero, the dynamics switch from being dominated by ω_{21} and ω_{43} to being dominated by ω_{32} and ω_{41}. At the transition point, the dynamics are governed by a combination of all four frequencies, giving the complex precession in Fig. 3(d).

The transition between the low- and high-k regimes can be understood by considering the eigenstates of $\hat{H}$. Because $V_R > V_I$, for illustrative purposes we consider a continuum version of $\hat{H}$ with only Rashba SOC, $\hat{H}_0 + \hat{H}_R = \hbar v_F \vec{\sigma}\cdot\vec{k} + \lambda_R(\vec{\sigma}\times\vec{s})$, where v_F is the Fermi velocity, $\vec{\sigma}$ are the pseudospin Pauli matrices, and λ_R is the Rashba strength. Assuming k along the zig-zag ($+x$) direction, the eigenstates at large k are $|\phi_j\rangle \approx [1 \;\; \nu_j \;\; i\zeta_j \;\; i\zeta_j\nu_j]^T$, where $\nu_j = -1(+1)$ for bands 1 and 2 (3 and 4), and $\zeta_j = -1(+1)$ for bands 2 and 3 (1 and 4). The spin polarization of each eigenstate is $(0, \zeta_j, 0)$ and the pseudospin polarization is $(\nu_j, 0, 0)$. Looking back at Eq. (4), the weights of the oscillating terms are then proportional to $\langle\phi_i|s_z|\phi_j\rangle = (1+\nu_i\nu_j)(1-\zeta_i\zeta_j)$. Thus, in the high-$k$ regime, precession only occurs between eigenstates with the same pseudospin and opposite spin, i.e., only between the two conduction bands (ω_{43}) and the two valence bands (ω_{21}). At small k, the Rashba term $\hat{H}_R$ dominates and the eigenstates become $|\phi_{1,4}\rangle \approx [0 \;\; \mp 1 \;\; i \;\; 0]^T$ and $|\phi_{2,3}\rangle \approx [1 \;\; 0 \;\; 0 \;\; \pm i]^T$. In this regime, spin-pseudospin coupling is strong, as the spin-up and spin-down components of each eigenstate are located entirely on opposite sublattices [18]. It is clear that the conduction/valence bands no longer overlap, while the overlap between bands 1 and 4 (2 and 3) dominate the spin dynamics.

Spin relaxation in graphene with SOC. As shown in Fig. 3, the spin dynamics strongly depends on k near the Dirac point, with much weaker dependence at higher k. Using Eq. (1), we can predict that spin relaxation should be fast near the Dirac point and slower at higher energies. Looking at Fig. 2, a strong anisotropy in the spin relaxation is also anticipated. Along the zig-zag direction, the precession frequency away from the Dirac point varies slowly but continuously with energy, indicating that τ_s should saturate to a constant value. However, along the armchair direction the precession frequency remains constant, suggesting that τ_s should diverge away from the Dirac point. For transport in all directions simultaneously, we must account for both energy broadening and the anisotropy in k. Similar to the single-direction cases, τ_s should be small near the Dirac point and increase at higher energies. However, at higher energies the spin precession also becomes strongly direction-dependent, resulting in increased dephasing due to the mixing in k and eventually leading to a decrease in τ_s.

To verify these qualitative predictions, numerical calculations of spin dephasing and relaxation are performed. We compute the time and energy-dependent spin polarization of an initial state $|\psi_0\rangle$ as [18]

$$\vec{p}(E,t) = \frac{1}{2}\cdot\frac{\sum_k[\langle\psi(t)|\vec{s}\delta(E-\hat{H})|\psi(t)\rangle + \text{h.c.}]}{\sum_k\langle\psi(t)|\delta(E-\hat{H})|\psi(t)\rangle}, \quad (5)$$

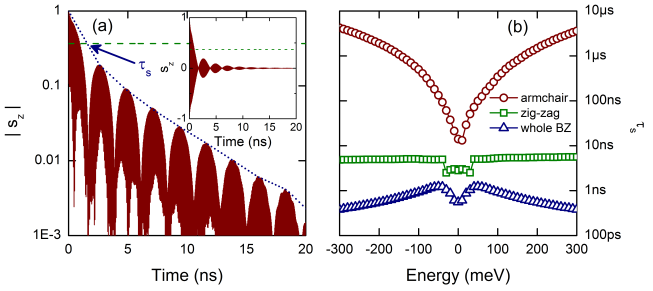

FIG. 4. (color online) Spin relaxation in graphene with SOC. (a) The spin dynamics at an energy of 100 meV reveal a complex behavior. (b) Energy-dependent spin relaxation time for various transport directions.

where $|\psi(t)\rangle = U(t)|\psi_0\rangle$, $U(t) = \sum_j |\phi_j\rangle\langle\phi_j|e^{-i\epsilon_j t/\hbar}$, $\delta(E-\hat{H}) = \sum_j |\phi_j\rangle\langle\phi_j|g(E-\epsilon_j)$, and g is a broadening function that can be Lorentzian, Gaussian, a Fermi distribution, etc. The sum represents a sample over k-space, and can be along a single direction or over the entire Brillouin zone. We extract τ_s from the time dependence of $\vec{p}(E,t)$ at each energy. As shown in Fig. 4(a), the dynamics is too complex to fit to a simple decaying cosine, as in Eq. (1). Instead, we define τ_s to be the time at which the envelope function of $\vec{p}(E,t)$ falls below e^{-1}.

Fig. 4(b) presents τ_s as a function of energy, considering transport along the zig-zag and armchair directions and in all directions simultaneously. A Lorentzian broadening with $\eta = 13.5$ meV is assumed, together with initial polarization along the z-axis. As seen in this figure, the numerical results confirm our qualitative predictions of τ_s. Along the armchair direction, τ_s diverges with increasing energy, reaching 4 μs at 300 meV. However, near the Dirac point the dephasing is still strong enough to limit τ_s to 14 ns. Along the zig-zag direction, τ_s saturates to 6 ns with a slightly lower value of 3 ns at the Dirac point. For transport in all directions, dephasing is much stronger due to the orientation dependence of the spin dynamics, giving τ_s between 380 ps and 1.2 ns. A characteristic "inverted-W" shape is observed with a high-energy downturn of $\tau_s(E)$ resulting from the increased anisotropy of the spin splitting, as pictured in Figs. 2(c) and (d).

Discussion and conclusions. Spin lifetime has been found to be dictated by dephasing effects, which result from the combination of energy broadening and nonuniform spin precession. Spin relaxation has been also shown to be highly anisotropic (Fig. 4), suggesting possible design of efficient graphene spintronic devices for instance by collimating the injected charge carriers [27]. In Fig. 4(b), τ_s exhibits a characteristic "inverted-W" shape as a function of energy when mixing over all directions of k. Although there is no momentum scattering in these calculations, this situation does qualitatively mimic the randomization of the momentum direction in a disordered system. Thus, the inverted-W shape of $\tau_s(E)$ should be preserved in presence of stronger impurity scattering [18, 25]. The results of Fig. 4 finally assume a Lorentzian broadening, which in the ballistic regime would be induced by scattering processes randomizing the phase of the electrons without strongly altering their momentum. We note that for all types of broadening $\tau_s \propto 1/\alpha$, meaning that the results of Fig. 4(b) scale linearly with the inverse of the Rashba SOC strength. For thermal broadening the spin lifetime is given by $\tau_s = 2.7/(\pi\alpha kT)$, which yields $\tau_s = 5.2$ ns for $kT = 13.5$ meV ($T = 160$ K).

Beyond graphene, the methodology and conclusions should be applicable to the understanding of spin dynamics in other Rashba SOC materials, including 2D electron gases [28], electronic excitations in 2D transition metal dichalcogenides [8], or Rashba-split surface states of topological insulators [29].

[1] Y.A. Bychkov and E.I. Rasbha, P. Zh. Eksp. Teor. Fiz. **39**, 66 (1984).

[2] S. Datta and B. Das, Appl. Phys. Lett. **56**, 665 (1990).

[3] J. Sinova, D. Culcer, Q. Niu, N.A. Sinitsyn, T. Jungwirth, and A.H. MacDonald, Phys. Rev. Lett. **92**, 126603 (2004).

[4] J. Sinova, S.O. Valenzuela, J. Wunderlich, C.H. Back, and T. Jungwirth, Rev. Mod. Phys., *in press*.

[5] A. Reynoso, G. Usaj, and C.A. Balseiro, Phys. Rev. B **73**, 115342 (2006).

[6] A. Manchon, H.C. Koo, J. Nitta, S.M. Frolov, and R.A. Duine, arXiv:1507.02408.

[7] C. Ertler, S. Konschuh, M. Gmitra, and J. Fabian, Phys. Rev. B **80**, 041405 (2009). D. Huertas-Hernando, F. Guinea, and A. Brataas, Phys. Rev. Lett. **103**, 146801 (2009). Y. Zhou and M.W. Wu, Phys. Rev. B **82**, 085304 (2010).

[8] H. Ochoa and R. Roldan, Phys. Rev. B **87**, 245421 (2013). L. Wang and M.W. Wu, Phys. Rev. B **89**, 115302 (2014). A. Kormanyos, V. Zólyomi, N.D. Drummond, P. Rakyta, G. Burkard, and V.I. Fal'ko, Phys. Rev. B **88**, 045416 (2013).

[9] D. Xiao, G.-B. Liu, W. Feng, X. Xu, W. Yao, Phys. Rev. Lett. 108, 196802 (2012).

[10] M. Gmitra and J. Fabian, arXiv:1506.08954.

[11] M.I. Dyakonov and V.I. Perel, Sov. Phys. Solid State **13**, 3023 (1972).

[12] P.G. Elliot, Phys. Rev. **96**, 266 (1954). Y. Yafet, *Solid State Physics*, eds. F. Seitz and D. Turnbull (Academic, New York, 1963), Vol. 13.

[13] H. Ochoa, A. H. Castro Neto, F. Guinea, Phys. Rev. Lett. **108**, 206808 (2012).

[14] H. Min, J.E. Hill, N.A. Sinitsyn, B.R. Sahu, L. Kleinman, and A.H. MacDonald, Phys. Rev. B **74**, 165310 (2006). D. Huertas-Hernando, F. Guinea, and A. Brataas, Phys. Rev. B **74**, 155426 (2006). Y. Yao, F. Ye, X.-L. Qi, S.-C. Zhang, and Z. Fang, Phys. Rev. B **75**, 041401 (2007). M. Gmitra, S. Konschuh, C. Ertler, C. Ambrosch-Draxl, and J. Fabian, Phys. Rev. B **80**, 235431 (2009). S. Konschuh, M. Gmitra, and J. Fabian, Phys. Rev. B **82**, 245412 (2010).

[15] N. Tombros, C. Jozsa, M. Popinciuc, H.T. Jonkman, and B.J. van Wees, Nature **448**, 571 (2007). C. Józsa, T. Maassen, M. Popinciuc, P.J. Zomer, A. Veligura, H.T. Jonkman, and B J. van Wees, Phys. Rev. B **80**, 241403 (2009). A. Avsar *et al.*, Nano Lett. **11**, 2363 (2011). W. Han and R.K. Kawakami, Phys. Rev. Lett. **107**, 047207 (2011). T. Maassen, J.J. van den Berg, N. IJbema, F. Fromm, T. Seyller, R. Yakimova, and B. J. van Wees, Nano Lett. **12**, 1498 (2012). I. Neumann, J. Van de Vondel, G.

Bridoux, M.V. Costache, F. Alzina, C.M. Sotomayor Torres, and S.O. Valenzuela, Small **9**, 156 (2013). M.H.D. Guimarães, P.J. Zomer, J. Ingla-Aynés, J.C. Brant, N. Tombros, and B.J. van Wees, Phys. Rev. Lett. **113**, 086602 (2014). M.V. Kamalakar, C. Groenveld, A. Dankert, and S.P. Dash, Nat. Commun. **6**, 6766 (2015).

[16] A.H. Castro Neto and F. Guinea, Phys. Rev. Lett. **103**, 026804 (2009).

[17] C. Weeks, J. Hu, J. Alicea, M. Franz, and R. Wu, Phys. Rev. X **1**, 021001 (2011).

[18] D.V. Tuan, F. Ortmann, D. Soriano, S.O. Valenzuela, and S. Roche, Nat. Phys. **10**, 857 (2014).

[19] D. Kochan, M. Gmitra, and J. Fabian, Phys. Rev. Lett. **112**, 116602 (2014).

[20] T. Butz, *Fourier Transformation for Pedestrians* (Springer International, Cham, Switzerland, 2006).

[21] G. Bevilacqua, arXiv:1303.6206.

[22] C.L. Kane and E.J. Mele, Phys. Rev. Lett. **95**, 226801 (2005).

[23] M. Zarea and N. Sandler, Phys. Rev. B **79**, 165442 (2009).

[24] R. van Gelderen and C.M. Smith, Phys. Rev. B **81**, 125435 (2010).

[25] D.V. Tuan *et al.*, *submitted*.

[26] B. Dlubak *et al.*, Nature **8**, 557 (2012).

[27] C.-H. Park, Y.-W. Son, L. Yang, M.L. Cohen, and S.G. Louie, Nano Lett. **8**, 2920-2924 (2008).

[28] S. LaShell, B.A. McDougall, and E. Jensen, Phys. Rev. Lett. **77**, 3419 (1996). Yu.M. Koroteev, G. Bihlmayer, J.E. Gayone, E.V. Chulkov, S. Blügel, P.M. Echenique, and Ph. Hofmann, Phys. Rev. Lett. **93**, 046403 (2004). C. Zhao, J. Li, Y. Yu, H. Ni, Z. Niu, and X. Zhang, Appl. Phys. Lett. **104**, 052411 (2014).

[29] E. Wang, P. Tang, G. Wan, A.V. Fedorov, I. Miotkowski, Y.P. Chen, W. Duan, and S. Zhou, Nano Lett. **15**, 2031 (2015).